Effect of Barium Doping on the Structure, Water Incorporation and Electrical Properties of Nano-crystalline Ceria

Bingxue Hou

School of Materials Engineering, Panzhihua University, Panzhihua Sichuan, China

416517865@qq.com

Abstract. A series of Ce1-xBaxO2-δ (x=0.0, 0.05, 0.10, 0.15 and 0.2) were synthesized by citrate-nitrate auto combustion method. More than 98% of theoretical density was obtained after sintering at 1400 ˚C for 5h. All compositions (x<0.1) were found to have the fluorite phase. The compositions (x>0.1) also contained the second phase BaCeO3. It was observed that composition Ce0.9Ba0.1O2-δ showed the higher ionic conductivity of 3×10-3 cm−1 at 700 °C among the series. The conductivity decreased with increasing x. This is due to the formation of second phase BaCeO3 and increasing probability of formation of neutral associated defect pairs.

Keywords: Solid oxide fuel cell; Electrolyte Ba-doped Ceria; Electrical Conductivity.

1. Introduction

Solid oxide fuel cell (SOFC) is one of the alternative technologies for the production of clean energy, promising high efficiencies and low environmental impact. SOFC offers great potential for the most cost-effective utilization of hydrocarbon fuels [1]. Yttria stabilized zirconia (YSZ) is a well-known electrolyte. However, YSZ must be operated at higher temperatures around 1000 ˚C in order to obtain higher oxygen ionic conductivity. Comparing with YSZ electrolytes, it has been revealed that ceria doped with divalent or trivalent cations [2-7] exhibit higher ionic conductivity at lower temperature (500 ˚C -700 ˚C).

Barium is known to volatize at high temperatures, forming amorphous barium oxide in the grain boundary regions, which can lower the total conductivity of the material [8-9]. However, dense barium cerate ceramics were found to be kinetically stable in CO2 over long periods of time, for example, week, because the chemical reactions that are involved are interfacial [8-10]. In the presence of high steam concentrations, barium cerate perovskites decompose to form Ba $(OH)_2$, CeO_2, and Y_2O_3, which reflects the high solubility of protons in the material. Thermodynamic studies suggested that the high hydration enthalpy of barium cerate is a consequence of the high basicity of barium [11]. Cheap barium (Ba^{2+}) element was incorporated into ceria in order to fully investigate the viability of $Ce_{1-x}Ba_xO_{2-\delta}$ when used as potential electrolytes for SOFC in the paper. This study is also concerned with the relationship between dopant concentration and properties such as water incorporation. Citrate-nitrate auto combustion method was used to obtain nano crystalline powders in the system $Ce_{1-x}Ba_xO_{2-\delta}$(x=0.0, 0.05, 0.10, 0.15 and 0.2).

2. Experimental

Powders with the general formula $Ce_{1-x}Ba_xO_{2-\delta}$ (x=0.0, 0.05, 0.10, 0.15 and 0.2) (CBO) were synthesized by citrate-nitrate auto combustion method. High purity cerium nitrate ($Ce(NO_3)_3 \cdot 6H_2O$) and barium nitrate ($Ba(NO_3)_2$) (Sinopharm Chemical Reagent Co., Ltd.) were used as starting materials. A stoichiometric amount of $Ce(NO_3)_3 \cdot 6H_2O$ and $Ba(NO_3)_2$ were mixed with the nitric acid. Citric acid was added to the above solution in 1.5:1 M ratio and ammonium hydroxide was added drop by drop to the solution to adjust pH (≈7). After the whole mixture was stirred at 40 ˚C, a homogeneous solution was then formed. The obtained gel placed in a ceramic burner started to foam, swell and finally burnt with glowing flints and the evolution of large amounts of gases occurred. This auto-ignition was completed within a few seconds giving rise to a light yellow colored ash, which the

auto-ignition temperature was nearly 1000˚C to obtain the most stable mixed oxide phase. Then the powders were claimed at 600 ˚C for 2 h to remove the carbonaceous materials. Synthesized powders were uniaxial pressed under a pressure of 8 MPa for 5 min. into a circular pellet using a stainless steel die of dimensions 12 mm in diameter and 2 mm in thickness, and then pellets were sintered in air at 1400 ˚C for 5 h with a programmed heating rate of 5 ˚C /min. Densities of the sintered samples were measured in water using Archimedes method and the calculated densities of sintered samples were found to be more than 98% of the theoretical density.

The prepared powders were directly characterized using XRD (Cu Kα radiation; D8 ADVANCE, Bruker Corporation, Germany) in the range of $20° \leq 2\theta \leq 80°$. XRD analysis was also performed on samples sintered in air at 1400 ˚C for 5 h. Lattice parameter was calculated by fitting the observed reflections with a least-square refinement UNIT CELL program. The particle size distribution of the powders was measured by laser diffraction (Malvern Rasterizer Hydro2000, Malvern Instruments Ltd. UK). The sintered pellets were polished, thermally etched and gold coated for microstructure analysis using the scanning electron microscope (JSM-6700F, JEOL, and Japan). To investigate the amount of water that can be incorporated in the different compositions, two typical as-prepared samples were first dried for 6 h and controlled atmosphere furnace at 1100 ℃. After cooling to room temperature, samples were immediately transferred into a Reuther thermo gravimetric analysis (TGA) instrument and heated at 5 ℃/min to 1000 ℃ in Ar atmosphere with the weight change recorded simultaneously.

AC impedance spectroscopy measurements were conducted by electrochemical impedance spectrum analyzer (CHI 600A, Chenhua Inc., Shanghai, PR China) in the frequency range from 0.01 to 100 kHz. The sintered CBO pellets (effective diameter: 11.11 mm; thickness: 1.4 mm) were coated with silver paste and fired at 800 ˚C for 1 h before measurement, and then were put into the tube furnace and heated at a heating rate of 2 ˚C min^{-1} in air. The conductivity measurements were carried out at different temperatures in the temperature range 300 ˚C-700 ˚C in 50 ˚C steps. Z-view software was used to analyze the impedance data and to calculate the grain, grain boundary and the total conductivity of the doped ceria samples. Silver paste was coated to each side of the sample, which was subsequently dried to produce solid silver electrodes on both sides of the pellet.

3. Results and discussion

The XRD patterns of CBO prepared powders are shown in Fig. 1. It shows that doped ceria powder crystallite had a single phase with cubic fluorite structure and were similar to pure ceria. However, from these figures, it is clear that a second phase $BaCO_3$ (JCPDS file no.005-626) was detected for compositions with x>0.1 in the present work. The reason is that excess amount of Ba^{2+} could easily react with CO_2 in the atmosphere. Fig.2 shows XRD patterns of CBO pellets sintered at 1400 ℃. Diffraction patterns were indexed on the basis of fluorite structure similar to CeO_2 using JCPDS powder file no.34-0394 and perovskite type of $BaCeO_3$ using JCPDS powder file no.022-074. It is observed that there was a second perovskite phase $BaCeO_3$ in addition to the fluorite phase for compositions with x>0.1. The introduction of Ba^{2+} into Ce^{4+} could cause a small shift in the ceria peaks. This shift is an indicative of variability in the lattice parameter. The lattice parameters and lattice volume of $Ce_{1-x}Ba_xO_{2-\delta}$ powders were calculated and summarized in Table 1. The reason was the difference in ionic radii of Ce^{4+} (0.97A) and Ba^{2+} (1.35A) in an oxide solid solution [12], respectively. Lattice parameter of Ba^{2+}-doped ceria samples is plotted as a function of mol% as shown in Fig. 3. It can be seen that lattice parameter increased with increasing the content up to 10 mol% and then decreased beyond 10 mol%. It indicates that the solubility of BaO in CeO_2 was between 5 and 10 mol%. This is in conformity with the results of powder XRD that show presence of second pervoskite $BaCeO_3$ phase. Pellets sintered at1400 ˚C for 5 h have densities more than 98% of theoretical values.

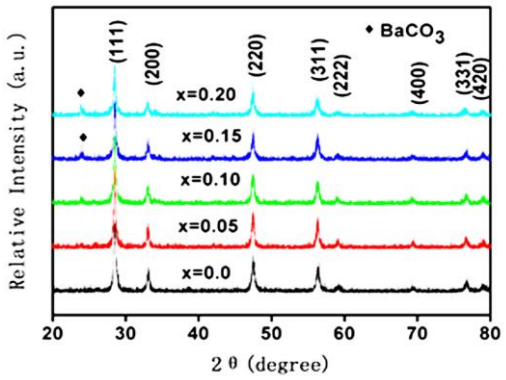

Fig.1 Powder X-ray diffraction patterns of various compositions of $Ce_{1-x}Ba_xO_{2-\delta}$ (x=0.0-0.2) powders.

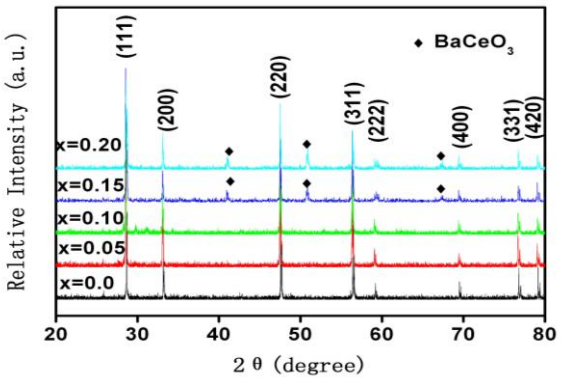

Fig.2 Powder X-ray diffraction patterns of various Compositions of $Ce_{1-x}Ba_xO_{2-\delta}$ (x=0.0-0.2) sintered at 1400 ℃.

Figure 4 shows the typical TEM micro-photographs of the CBO (x=0.1) powder. It can be clearly seen that nano-sized CBO crystals formed with uniform size and compact distribution. The observed crystalline grains for the CBO were of hexagonal shape with corners and edges, and then compacted with each other. The selected area electron diffraction pattern (SAED) exhibited eight broad rings which might be attributed to (1 1 1), (2 0 0), (2 2 0), (3 1 1), (2 2 2), (4 0 0), (3 3 1), and (4 2 0) reflections of the cubic fluorite structure of CeO_2, respectively, which were in accordance with the XRD pattern results.

Fig.5 shows the particles size distribution of prepared $Ce_{1-x}Ba_xO_{2-\delta}$ (x=0.0, 0.05, 0.10, 0.15 and 0.2) powders after ball-milling for 24h. It is observed that the particle size parameters d (0.5) of CBO powders were 1.647μm, 0.804μm, 0.426μm, 0.413μm, and 0.303μm, respectively. This suggests that some of agglomerates had been separated effectively, especially for $Ce_{1-x}Ba_xO_{2-\delta}$ (x=0.1-0.2) powders. It is shown that powders prepared by citrate-nitrate auto combustion method disperse very well and there are no sticky agglomerates. Particle sizing, however, using laser diffraction is very useful since it gives a quick and easy access to measurement of particle size.

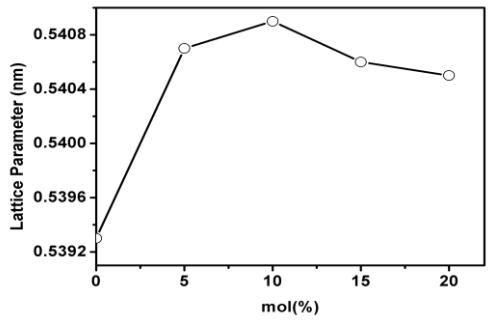

Fig.3 Variation of lattice parameter as function of the dopant concentration for the system $Ce_{1-x}Ba_xO_{2-\delta}$.

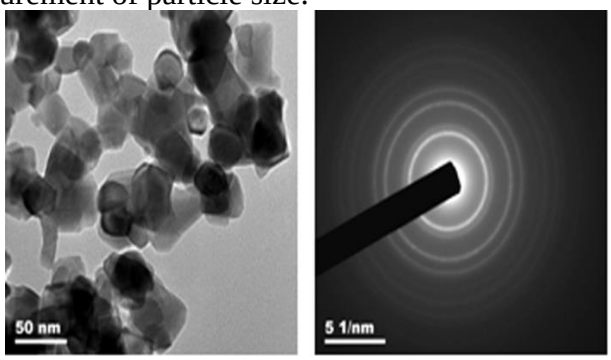

Fig.4 Typical TEM of the $Ce_{1-x}Ba_xO_{2-\delta}$ (x=0.1) powders.

Thermo gravimetric analysis (TGA) measurements were performed to determine the relative H_2O content in the structure. Fig.6 shows the weight changes during dehydration of typical $Ce_{1-x}Ba_xO_{2-\delta}$ (x=0.0, x=0.1) samples. It can be clearly seen that TGA analysis on $Ce_{1-x}Ba_xO_{2-\delta}$ (x=0.1)samples in air showed a mass loss of 1.60% occurs during heating from room temperature to 1000 ℃, while the $Ce_{1-x}Ba_xO_{2-\delta}$ (x=0.1)sample only showed a mass loss of 0.30%. The variation may imply that water uptake depended predominantly on the number of the dopant concentration. The variation of the maximum amount of water that could be incorporated into the structure at different dopant contents. The compositional region where water uptake is reduced is identical with that where the unit cell parameters deviate from their general trends reflecting that water incorporation has direct consequences on structural distortions.

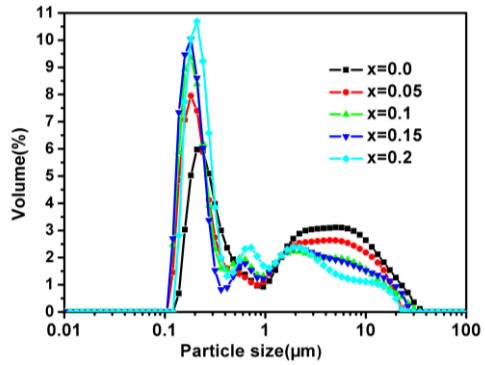

Fig.5 Particle size distribution for $Ce_{1-x}Ba_xO_{2-\delta}$ (x=0.0-0.2) powders.

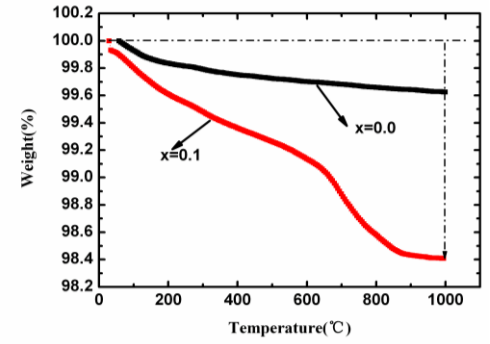

Fig.6 TGA traces for dehydrated $Ce_{1-x}Ba_xO_{2-\delta}$(x=0.0, 0.1) samples on heating in Ar.

Fig.7shows SEM surface photograph of $Ce_{0.9}Ba_{0.1}O_2$ sample sintered at 1400 ℃ and it is clear that the sample surface showed good densification. Few pores were present on the surface of the sample, which is in accordance with the relative density of the sintered pellets.

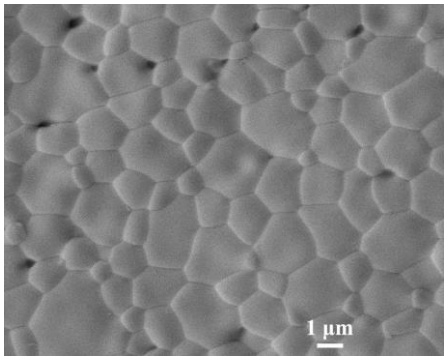

Fig.7 SEM surface micrograph of $Ce_{1-x}Ba_xO_{2-\delta}$ (x=0.1) sample sintered at 1400 ℃.

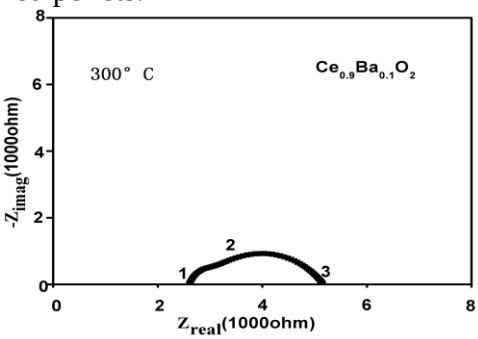

Fig.8Impedance plots for the composition $Ce_{1-x}Ba_xO_{2-\delta}$ (x=0.1) at 300 ℃

Fig.8 shows the typical impedance plots of $Ce_{0.9}Ba_{0.1}O_2$ at 300 ℃. It can be seen that arc corresponding to contribution of electrode polarization appears at 300 ℃. It points out that arcs 1, 2, and 3 responded to the grain interior, grain boundary, and the polarization of electrodes, respectively.

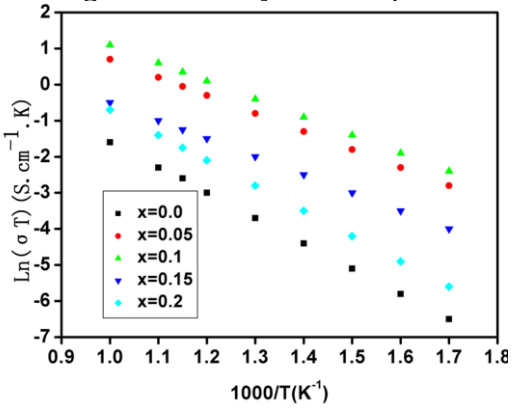

Fig.9 Relationship between conductivity and temperature for $Ce_{1-x}Ba_xO_{2-\delta}$ (x=0.0-0.2).

Fig.9shows Arrhenius plots of the total ionic conductivity for the $Ce_{1-x}Ba_xO_{2-\delta}$ (x=0.0, 0.05, 0.10, 0.15 and 0.2) (CBO) samples in the form of ln (σT) versus 1000/T. These plots are linear with single slope in the entire temperature range of measurement. For $Ce_{1-x}Ba_xO_{2-\delta}$(x=0.0, 0.05, 0.10, 0.15 and 0.2), the conductivity increased from x=0.0 to x=0.1 then decreased. It is noted that composition with x=0.1 exhibited the highest conductivity among all the compositions.

4. Conclusion

A series of $Ce_{1-x}Ba_xO_{2-\delta}$ with $0 \leq x \leq 0.2$ were synthesized by citrate-nitrate auto combustion method. Single phase formed in the compositions with $0 \leq x \leq 0.1$ at as low temperature as 600 ˚C. All compositions with $x>0.1$ contain second phase $BaCeO_3$ along with the major fluorite phase. More than 98% of theoretical density was obtained after sintering at 1400 ˚C for 5h. It was observed that composition $Ce_{0.9}Ba_{0.1}O_{2-\delta}$ showed the higher electrical conductivity of 0.0030 S cm^{-1} at 700 ℃ among the series. The electrical conductivity decreased with increasing x. This is due to the formation of second phase $BaCeO_3$ and increasing probability of formation of neutral associated defect pairs. Although the electrical conductivity, this makes it a potential candidate as a solid electrolyte being used in direct hydrocarbon solid oxide fuel cell.

Acknowledgment

The authors thank the Project (Serial number: 0290100238) for their financial support.

References

[1] Singhal, S. C. Advances in solid oxide fuel cell technology. Solid State Ionics 2000; 135, p. 305-13.

[2]A. S. Nowick, Mahan, W. L. Roth, Super ionic Conductors, Plenum, New York, 1976, p.395-412.

[3]C. B. Chounhary, H. S .Maiti, E. C. Subbara, Subbarao, Solid Electrolytes and their Applications, Plenum, New York, 1980, p.1-80.

[4]B. C. H. Steele. “Materials for IT-SOFC stacks 35 years R&D: the inevitability of gradualness?” Solid State Ionics 2000; 129, p.95-110.

[5]S. W. Zha, C. R. Xia, G. Y. Meng. Effect of Gd (Sm) doping on properties of ceria electrolyte for solid oxide fuel cells. J. Power Sources 2003; 115, p. 44-48.

[6]S. Kuharuangrong. Ionic conductivity of Sm, Gd, Dy and Er-doped ceria. J. Power Sources 2007; 171, p.506-510.

[7]H.Naba, H. Tawaga, Ceria-based solid electrolytes. Solid State Ionics 1996; 83: 1-16.

[8] Chen F., O. T, Meng G., Peng D. J. Mater. Chem. 1997; 3, p. 481.

[9] Haile S. M, Staneff G., Ryu K. H. J. Mater. Sci. 2001; 36, p.1149.

[10] Taniguchi N, Yasumoto E, Gamo T. J. Electrochem. Soc. 1990; 137, p.462.

[11] Kreuer K. D, Dippel T., Baikov Y. M., Maier J. Water solubility, proton and oxygen diffusion in acceptor doped BaCeO3: A single crystal analysis. Solid State Ionics 1996; 86, p.613.

[12] Shannon RD. Acta Cryst A 1976; 32, p.751.